possible to say at the moment whether or not the differences between theory and experiment are really significant when experimental error is taken into account.

ACKNOWLEDGMENTS

The author wishes to thank C. Elbaum and J. H. Weiner for helpful discussions and for critical reading of the manuscript.

PHYSICAL REVIEW VOLUME 188, NUMBER 3 15 DECEMBER 1969

ENDOR Study of a ⟨111⟩ Interstitial Defect in LiF†‡

Y. Hou Chu and Robert Lee Mieher*
Department of Physics, Purdue University, Lafayette, Indiana 47907
(Received 4 March 1969)

Results of (electron-nuclear double-resonance) measurements and analysis of a ⟨111⟩-oriented defect in pure LiF are presented. This paramagnetic defect is produced at low temperatures by x-ray or electron irradiation. The ENDOR hyperfine constants from 11 nonequivalent sets of lattice nuclei have been obtained by fitting the ENDOR spectrum to a spin Hamiltonian. Results of this ENDOR study show that this ⟨111⟩ defect is equivalent to an interstitial fluorine atom that has the form of a negatively charged diatomic molecule F_2^-, centered on a negative-ion site, with its molecular axis oriented along a ⟨111⟩ direction.

I. INTRODUCTION

THE intrinsic interstitial defect is one of the most fundamental of defects in solids. Various phenomena, especially in the area of radiation damage,[1] have been associated with the interstitial in various forms. However, direct observation and subsequent determination of the exact configuration or structure of the interstitial defect has been difficult. The interstitial may be a single atom or ion in a true interstitial position (i.e., point defect), or it may combine with lattice ions, in which case the interstitial nature is spread over more than one simple lattice position.

More complex interstitial-type defects exist, but their exact configurations are at most speculative. In pure metals the major radiation damage produced by low-temperature electron bombardment is thought to be interstitials and vacancies. Most information in metals has been obtained by measuring the recovery of the electrical conductivity during thermal annealing. Interpretation of this data has not yet yielded a unanimously acceptable model for even the simplest defects.[2] In semiconductors it is now established that radiation produced defects are primarily impurity-associated complexes. The simple vacancy and divacancy in Si are known to exist, but it is uncertain whether or not the pure interstitial is stable.[3] Watkins has observed and analyzed the ESR of electron-damaged Al-doped Si in terms of an Al^{++} interstitial. The growth of the ESR of the Al^{++} interstitial is similar to that of the vacancy defect. The Si interstitial, which is apparently mobile at helium temperature, displaces a substitutional impurity into an interstitial position. Simple defects in other semiconductors have not yet been identified.

Considerable interest in the study of interstitials in the alkali halides has developed in recent years.[4] One reason is that interstitials are complementary to the well-known and much studied F-type centers, which involve negative-ion vacancies. A second reason is the general improvement in crystal growing techniques, which allows the content of the specimen to be more closely controlled. Unknown or unwanted impurities often form associated defects in direct competition with intrinsic defects.

The relatively large ratio of α centers (a negative-ion vacancy) to F centers (an electron trapped at a negative-ion vacancy) concentration that is present after x irradiation at 4.2°K has been attributed to a nearby interstitial halide ion that retards electron trapping by the α center.[5] An optical-absorption band has been observed in electron-irradiated LiF at 77°K which has been attributed to the interstitial Li atom.[6]

† Work supported in part by the National Science Foundation, under Grant Nos. NSF-GP-04860 and NSF-GP-07779, and by the Advanced Research Projects Agency.

‡ Partially based upon a thesis submitted by Y. H. Chu for the Ph.D. degree at Purdue University.

* Alfred P. Sloan Foundation Fellow.

[1] For a recent review of radiation damage studies in metals and semiconductors, see J. W. Corbett, *Solid State Physics* (Academic Press Inc., New York, 1966), Suppl. 7.

[2] A. Sosin, in *Lattice Defects and Their Interpretations*, edited by R. R. Hasiguti (Gordon and Breach, Science Publishers, Inc., New York, 1967), p. 235.

[3] G. D. Watkins, *Radiation Damage in Semiconductors* (Academic Press Inc., New York, 1965), p. 97.

[4] For a review of color centers, see J. H. Schulman and W. D. Compton, *Color Centers in Solids* (Pergamon Publishing Corp., New York, 1962); *Physics of Color Centers*, edited by W. B. Fowler (Academic Press Inc., New York, 1968).

[5] F. Luty, *Haibleiter Probleme* (Frederick Vieweg und Sohn, Brauschweig, Germany, 1961), Vol. 6, p. 238.

[6] Y. Farge, M. Lambert, Compt. Rend. **258**, 5199 (1964); Proceedings of the International Symposium on Color Centers, Rome, 1968 (unpublished).

It has been established that the defects that are responsible for some of the optical V bands are related to interstitials. This is based on the observation that a definite relationship exists between the V bands and the H bands,[7] which has been attributed to the interstitial halogen atom. For instance, in KCl it is possible to produce the H band by optically bleaching the V_1 band at helium temperature.[8] In addition to the V and H bands, another optical absorption in the ultraviolet has been labeled the H' band. The H' center may also involve interstitials, since it was found that the sum of the H' and H centers was proportional to the numbers of F center.[9]

The identification of the H band as the interstitial halogen atom is based on an ESR study of x-rayed KCl, KBr, and LiF by Känzig and Woodruff.[10] They called their defect the H center, since it appeared to correspond to the optical H band, although the H band in LiF has not been identified. The interstitial halogen took the form of a negatively charged diatomic molecule (e.g., F_2^-) that was situated on a single negative-ion lattice site and oriented along a ⟨110⟩ axis. In a recent ENDOR experiment, it was shown that the ⟨110⟩ H center in LiF is actually associated with a Na^+ ion impurity that is located on a nearest-neighbor Li^+ ion site.[11] It is still possible that the ⟨110⟩ H-center defects in KCl and KBr are intrinsic. Nevertheless, it must be noted that in KCl, the V_1 center, which can be optically converted into the ⟨110⟩ H-center defect,[8] is now believed to involve the Na^+ impurity.[12]

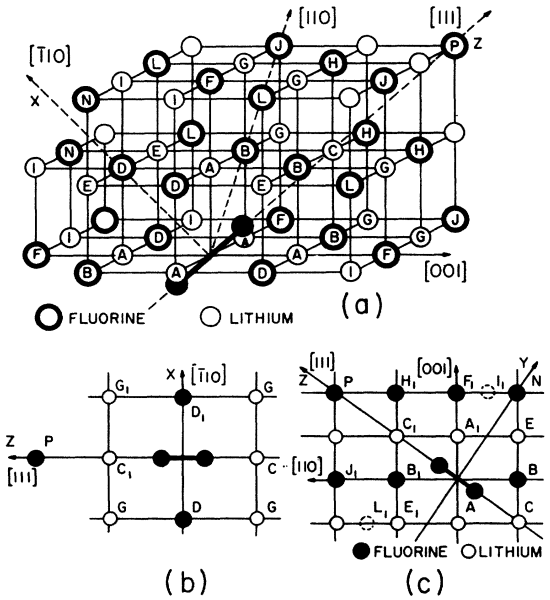

FIG. 1. The ⟨111⟩ defect. (a) Lattice model. Lattice nuclei which are located in the (b) (1̄12) and (c) (110) planes.

We present here the evidence for the existence of a "pure" interstitial defect in LiF. We have produced by low-temperature x-ray and electron irradiation of pure LiF a new paramagnetic defect with ⟨111⟩ symmetry.[13] Results of ESR and ENDOR measurements show that the interstitial defect has the configuration of an F_2^- molecule ion that is situated on a single negative-ion site. The ⟨111⟩ defect model and surrounding lattice are shown in Fig. 1. The neighboring lattice nuclei are labeled according to ENDOR shells and will be discussed later. The results of our ESR measurements have been presented earlier.[13] In this paper, results of our ENDOR measurements are presented.

The idea of a ⟨111⟩ defect is not new. This model has been proposed for the optical V_4 band in KBr.[14] Impurity associated defects such as the FCl^- in alkali halides[15] that are oriented along ⟨111⟩ have been studied. The R center (three coplanar F centers that are located on the points of an equilateral triangle) also has ⟨111⟩ symmetry.[16] In metals, the split interstitial model is closely related to the ⟨111⟩ defect.

Rabin and Klick have shown that the rate of production of F centers is directly related to the ease in fitting a halogen ion into the interstitial position along a ⟨110⟩ axis.[17] On this basis, the ⟨111⟩ orientation of the interstitial might be favored over the other crystal directions, since in LiF there appears to be less crowding in the ⟨111⟩ direction.[13] Dienes *et al.* have made energy calculations for the interstitial defect with ⟨111⟩ and ⟨110⟩ symmetry in KCl and NaCl.[18] They have shown that the ⟨111⟩ orientation may be more favorable if only electrostatic, core repulsion, and polarization terms are considered.

II. EXPERIMENT

All measurements were taken on high-purity single-crystal LiF (from Harshaw). Sample dimensions were $\frac{1}{4}\times\frac{1}{4}\times\frac{3}{4}$ in. with the long axis along a ⟨110⟩ axis. By rotating the sample about the long dimension, the dc magnetic field $\mathbf{H}_0$ is contained in a {110} plane. The sample was mounted at the end of a copper finger that was attached to the helium container of a double Dewar (Hofman model HLOR). Temperatures were measured by a calibrated carbon resistor that was imbedded near the sample in the copper finger. Since

[7] W. H. Duerig and J. J. Markham, Phys. Rev. **88**, 1043 (1952).
[8] C. J. Delbecq, J. L. Kolopus, E. L. Yasaitus, and P. H. Yuster, Phys. Rev. **154**, 866 (1967).
[9] B. J. Faraday and W. D. Compton, Phys. Rev. **138**, A893 (1965).
[10] W. Känzig and T. O. Woodruff, J. Phys. Chem Solids **9**, 70 (1958)
[11] M. L. Dakss and R. L. Mieher, Phys. Rev. Letters **18**, 1056 (1967); Phys. Rev. **187**, 1067 (1969).
[12] J. L. Kolopus, C. J. Delbecq, E. L. Yasaitus, and P. H. Yuster, Bull. Am. Phys. Soc. **10**, 1110 (1965).
[13] Y. H. Chu and R. L. Mieher, Phys. Rev. Letters **20**, 1289 (1968).
[14] J. D. Kingsley, J. Phys. Chem. Solids **23**, 949 (1962).
[15] J. W. Wilkins and J. R. Gabriel, Phys. Rev. **132**, 1950 (1963).
[16] H. Seidel, Phys. Letters **7**, 27 (1963).
[17] H. Rabin and C. C. Klick, Phys. Rev. **117**, 1005 (1960).
[18] G. J. Dienes, R. D. Hatcher, and R. Smoluchowski, Phys. Rev. **157**, 692 (1967).

the resistor was located between the sample and the helium bath, the sample temperature is expected to be slightly higher than that indicated by the resistor. Nevertheless, all temperatures will be those measured by the resistor.

Measurements were made on an X-band superheretodyne ENDOR spectrometer operating at 8830 Mc/sec. ENDOR was observed using the Seidel method (stationary ENDOR).[19] Since the spectrometer is the same one used previously to measure the ENDOR of the V_K center in LiF,[20] spectrometer details and experimental techniques will not be discussed here.

The ⟨111⟩ defect has been produced by x-ray[21] or electron[22] irradiation at temperatures between 4.2 and 40°K. Presumably, this defect could be produced at higher temperatures close to the bleaching temperature of about 60°K. During and after the irradiation, the sample was exposed only to weak infrared light. The production of defects by x rays is slow, but the rate appears to be constant. About 40 and 300 h of irradiation are required to take ESR and ENDOR measurements, respectively.

Defect production by electron bombardment is more efficient. Roughly twice as many defects are present after 3 h of electron irradiation as there are present after 300 h of x irradiation. The ⟨111⟩ defect has also been produced by electron irradiation in LiF which was doped with 1% NaF in the melt. In the doped sample the ⟨110⟩ H center is also produced. The ratio of ⟨110⟩ H center to ⟨111⟩ defect concentration was about 5 to 1. Roughly 30 times as many ⟨111⟩ defects are produced in the pure LiF as in the doped LiF for 3 h of electron irradiation. The temperature during the electron irradiation ranged between 20 and 40°K. ESR has been observed from liquid-helium temperature to about 50°K. Throughout this study, the ⟨110⟩ defect was not observed in the pure LiF. Dakss and Mieher produced the ⟨110⟩ defect by x raying reagent-grade LiF at liquid-nitrogen temperature.[11] Also, they observed no ⟨110⟩ defects after 100-h irradiation of pure Harshaw LiF at liquid-nitrogen temperature.

The fact that the production rate is constant and the production has not been observed to saturate suggests that the defect is intrinsic and that impurities are not involved in the production mechanism. The V_K center[20,23] is also formed, but its production begins to saturate after about 100 h of x irradiation. The formation of the V_K center, or self-trapped hole, involves the removal of an electron from a lattice halide ion and the subsequent localization of the hole on two adjacent lattice halide ions. Any available electron traps that are initially present (e.g., impurities or vacancies) would be quickly filled in the V_K formation process, since the V_K center involves only electronic displacement and not ionic displacement. The F center is also produced, and its production rate does not appear to saturate. It is possible that the ⟨111⟩ defect and the F centers are produced in pairs. Since the ⟨111⟩ defect is morphologically equivalent to the ⟨110⟩ defect as proposed by Känzig and Woodruff, the various mechanism schemes that have been suggested for the H- and F-center production should also apply to the ⟨111⟩ defect and F center.[24] Our ENDOR results show that the ⟨111⟩ defect is not located within several lattice sites of any other defect.

III. ELECTRON SPIN RESONANCE

The ESR of the F_2^--type defects (e.g., V_K, V_{KA}, H) in alkali fluorides are all very similar. Before discussing the ENDOR of the ⟨111⟩ defect, it is beneficial to review the salient features of the ESR of F_2^--type defects.[25] The spectrum of the ESR is characterized by the large anisotropic hyperfine interaction between the unpaired electron and the two fluorine nuclei of the molecule ion. The spectrum of the ESR is composed of four resonance lines with the separation between the outermost lines being about 1800 G. The separation between the middle two lines is usually too small for the lines to be resolved, except when the magnetic field approaches the plane perpendicular to the molecular axis. Experimentally, the F_2^- possesses axial symmetry about the molecular axis, although the ⟨110⟩-oriented defects have orthorhombic or lower symmetry. It is therefore possible to characterize the ESR angular dependence by a single angle ξ which $\mathbf{H}_0$ makes with the molecular axis. The ⟨111⟩ defect, which has rhombohedral symmetry, is rigorously axially symmetric. In the following discussion the two fluorines of the molecule ion will be called the ESR fluorines, and their interaction with the unpaired electron will be called the ESR hyperfine interaction.

The spin Hamiltonian for the F_2^- defect can be written

$$\mathcal{H}=\beta_0\mathbf{S}\cdot\mathbf{g}\cdot\mathbf{H}_0+g_0\beta_0\mathbf{K}\cdot\mathbf{T}\cdot\mathbf{S}-\gamma_F h\mathbf{K}\cdot\mathbf{H}_0 +\sum_n(h\mathbf{I}_n\cdot\mathbf{A}_n\cdot\mathbf{S}-\gamma_n h\mathbf{I}_n\cdot\mathbf{H}_0), \quad (1)$$

[19] H. Seidel, Z. Physik **165**, 218 (1961); **165**, 239 (1961).

[20] R. Gazzinelli and R. L. Mieher, Phys. Rev. Letters **12**, 644 (1964); Phys. Rev. **175**, 395 (1968).

[21] Norelco MG150 x-ray tube; tube voltage, 75 keV; tube current, 30 mA; sample position, 9 mm from target with 3-mm Al inherent filtration plus ½-mm quartz and ½-mm Al_2O_3 (General Electric Lucalox).

[22] The electron irradiations were performed on Professor MacKay's 4.5-MeV linear electron accelerator for which we wish to acknowledge his cooperation and assistance. The electron current on the sample ranged between 0.25 to 0.5 μA.; 1-mil titanium filtration plus quartz and Al_2O_3 as in Ref. 21.

[23] T. G. Castner and W. Känzig, J. Phys. Chem. Solids **3**, 178 (1957); T O. Woodruff and W. Känzig, J. Phys. Chem. Solids **5**, 268 (1958).

[24] See, e.g., C. C. Klick, Phys. Rev. **120**, 760 (1960); R. E. Howard, S. Vosko, and R. Smoluchowski, Phys. Rev. **122**, 1406 (1961); see also Refs. 9 and 10

[25] For a thorough discussion of the ESR of the V_K center see Ref. 23. For a derivation of the ESR spin Hamiltonian, see C. P. Slichter, *Principles of Magnetic Resonance* (Harper and Row Publishers, Inc., New York, 1963). See also T. N. Casselman and J. J. Markham, J. Chem. Phys. **42**, 4178 (1965).

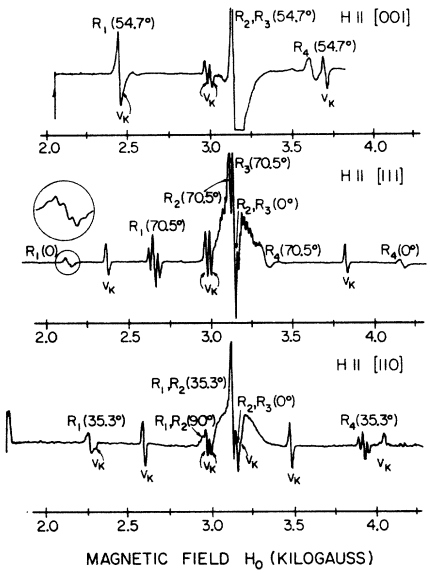

FIG. 2. The absorption spectra of the ESR are shown at about 40°K after 300 h of x irradiation for $\mathbf{H}_0$ parallel to the three crystal directions. The V_K, F, and ⟨111⟩ defects are present as well as an additional defect with much weaker intensity. The resonance lines of the ⟨111⟩ defect are indicated by $R_i(\xi)$ (see text). The insert for the [111] spectrum shows the secondary splitting.

where $\mathbf{S}$, $\mathbf{K}$, and $\mathbf{I}_n$ are the electron spin, effective nuclear spin of the ESR fluorines, and nuclear spin of the nth lattice nucleus, respectively. The units are G ($\mathbf{T}$), Mc/sec ($\mathbf{A}_n$), and Mc/sec G (γ). The summation includes all neighboring lattice nuclei. The last term represents the hyperfine interaction between the paramagnetic electron and the lattice nuclei, and is responsible for the inhomogeneous broadening of the ESR line. It is this broadening that is resolved by the ENDOR technique.[26]

In Fig. 2 is shown the spectrum of the ESR for $\mathbf{H}_0$ along the three symmetry axes of the crystal. The

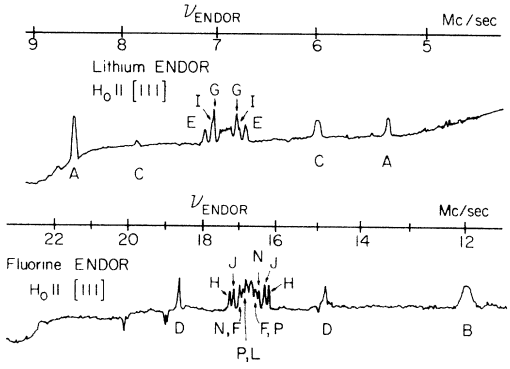

FIG. 3. The absorption spectra of the lithium and fluorine ENDOR are shown for $\mathbf{H}_0$ parallel to [111]. The ENDOR was taken at about 40°K after 300 h of x irradiation. The ENDOR signal observed after 3-h electron bombardment was about twice as large.

[26] G. Feher, Phys. Rev. **105**, 1122 (1957); **114**, 1219 (1959).

ESR constants were found to be $g_X=g_Y=2.0105$, $g_Z=2.0017$, $T_X=T_Y=19.0$ G, and $T_Z=1005.9$ G. The absorption lines of the ⟨111⟩ defect have been labeled according to the notation of Woodruff and Känzig.[23] The resonance lines R_1 to R_4 are labeled in the order of occurrence as $\mathbf{H}_0$ is increased from a low to a high field. For $\xi \lesssim 75°$, R_1 to R_4 can be associated with the ESR fluorine nuclear states $|K,m_K\rangle = |1,1\rangle$, $|1,0\rangle$, $|0,0\rangle$, and $|1,-1\rangle$, respectively. Secondary splitting can be observed for certain ESR lines. This secondary splitting is complicated because the principal axes of the hyperfine interaction responsible for the splitting does not coincide with the principal axes of the molecular ion. Also, this structure depends on the ESR fluorine nuclear state $|K,m_k\rangle$. Because of this behavior, we have not attempted to determine values for the components of this $\mathbf{A}$ from the ESR. This secondary splitting will be discussed later, after we discuss the ENDOR of the fluorine B nuclei.

IV. ENDOR

A. General

On the basis of the ESR measurements alone, it was possible to propose a model for the ⟨111⟩ defect with a high degree of certainty. However, it is known that the effect of the lattice on the wave function of an F_2^--type defect is small. The resolution of ESR is too low to rule out the possibility of impurity association. The ENDOR technique makes possible the study of the hyperfine interactions of many neighboring lattice nuclei and effectively increases the resolution by several orders of magnitude.

For the F_2^- type defects, ENDOR hyperfine constants normally can be obtained by taking ENDOR data on only one of the four ESR lines.[20,27] Although the ENDOR from the R_4 line was generally stronger than that from the R_1 line, the presence of the F center did not permit measurement of R_4 when the angle between $\mathbf{H}_0$ and the plane perpendicular to the molecular axis was less than 30°. Therefore, ENDOR data were taken on both the R_1 and R_4 lines.

Typical recorder graphs of the Li and F ENDOR are shown in Fig. 3. ENDOR lines from 13 nonequivalent lattice shells have been observed. In Figs. 4 and 5 the angular dependence of the ENDOR spectra for the magnetic field rotated in the $(\bar{1}10)$ plane are shown. Rather than the measured ENDOR frequency ν, the normalized frequency $\nu-\gamma_n\mathbf{H}_0$ is plotted (see Sec. IV B). The linewidth of the ENDOR of the nearest-neighbor fluorines (shell B) was broader ($\approx$200 versus 40 kc/sec) than the linewidth of the other lattice nuclei. The ENDOR from shell B could not be followed over the full angular rotation, because of the extreme line broadening and the strong angular dependence. The measured frequency ν is plotted in Fig. 6 for the shell

[27] D. F. Daly and R. L. Mieher, Phys. Rev. **175**, 412 (1968).

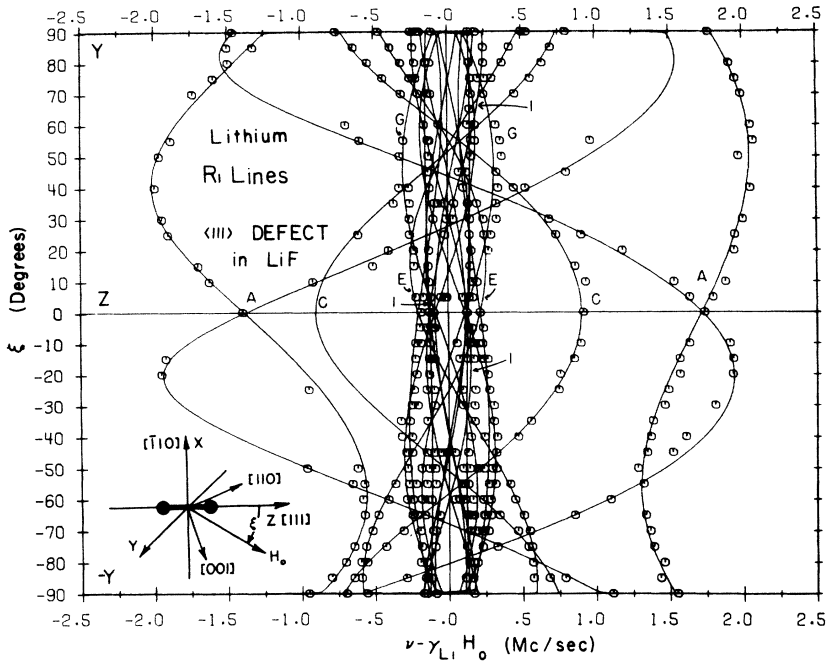

FIG. 4. Plot of the experimental and fitted angular dependence of the lithium ENDOR spectrum taken on the R_1 ESR line. In Figs. 4–7 not all of the experimental points have been plotted.

B fluorines, since the hyperfine interaction is greater than the free nuclear Zeeman interaction $\gamma_n \mathbf{H}_0$. The calculated angular dependence of the ENDOR of the R_3 ESR line, which is not affected by the ESR hyperfine interaction, is also shown for comparison. The intensity of the ENDOR signal depends both on the choice of ESR line and the orientations of the magnetic field with respect to the axis of the molecule ion. As ξ approached $\pm 90°$, the signals weakened considerably.

The dependence of the spectrum of the ENDOR on the choice of ESR line is shown in Fig. 7 for the shell A lithium nuclei. This variation with the ESR

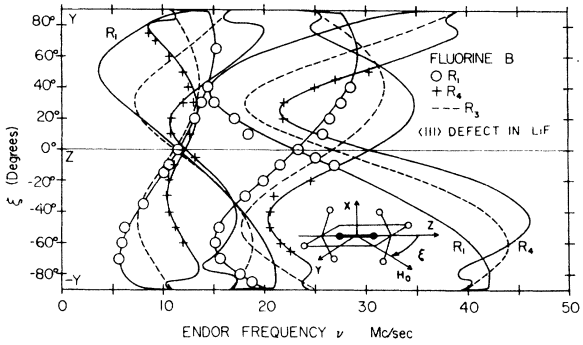

FIG. 6. Plot of the angular dependence of the fluorine B ENDOR spectrum.

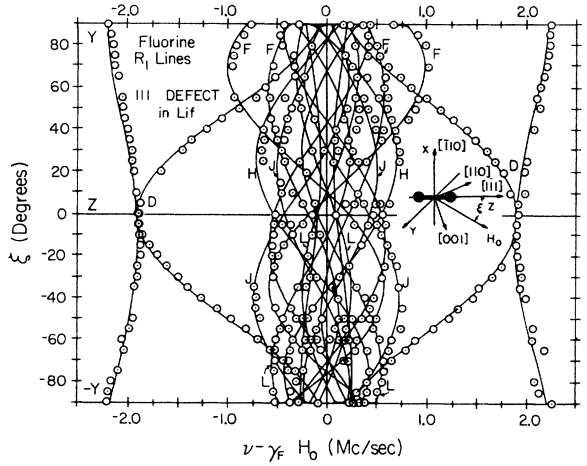

FIG. 5. Plot of the angular dependence of the fluorine ENDOR spectrum taken on the R_1 ESR line.

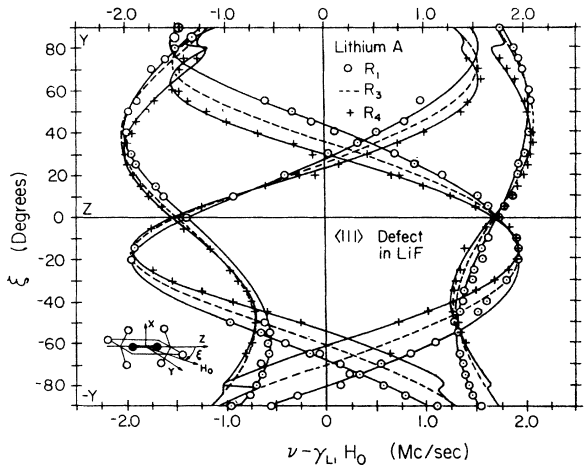

FIG. 7. Plot of the angular dependence of the lithium A ENDOR spectrum.

lines is due to the large anisotropic ESR hyperfine interaction.[20,27,28]

B. Spin Hamiltonian

The spin Hamiltonian that is used to analyze the spectra of the ENDOR was given in Eq. (1). Because the hyperfine interactions of the lattice nuclei are small[29] and quadrupole interactions are zero or unresolved, it is possible to treat each lattice nucleus separately [i.e., remove the summation in Eq. (1)] and to let $\mathbf{I}_n=\frac{1}{2}$. This spin Hamiltonian has been used successfully to determine ENDOR hyperfine constants for several F_2^--type defects in alkali fluorides.[11,20,27,28]

There are two contributions to the ENDOR hyperfine tensor $\mathbf{A}$:

$$\mathbf{A}=\mathbf{B}+a\mathbf{1}. \tag{2}$$

The tensor $\mathbf{B}$, which represents the dipole-dipole hyperfine interaction between the unpaired electron and a lattice nucleus, has the components

$$B_{ik}=\gamma_e\gamma_n h^2\int\left(\frac{3x_ix_k-r^2\delta_{ik}}{r^5}\right)|\psi(r)|^2dV. \tag{3}$$

$\mathbf{B}$ is symmetric and traceless.

The last term in Eq. (2) is the Fermi contact interaction

$$a=(8\pi/3)\gamma_e\gamma_n h^2|\psi(0)|^2, \tag{4}$$

and is a measure of the total unpaired spin density at the ENDOR nucleus.

ENDOR experiments in alkali halides normally result in a determination of the principal-axes values of $\mathbf{A}$, $\mathbf{A}_x$, $\mathbf{A}_y$, and $\mathbf{A}_z$, for each set of nonequivalent lattice nuclei. Since $\mathbf{B}$ is traceless, both a and the principal values of $\mathbf{B}$, $\mathbf{B}_x$, $\mathbf{B}_y$, and $\mathbf{B}_z$ are known once the components of $\mathbf{A}$ are determined:

$$a=\tfrac{1}{3}\sum_i \mathbf{A}_i, \quad \mathbf{B}_i=\mathbf{A}_i-a \quad (i=x,y,z). \tag{5}$$

The principal axes of $\mathbf{A}$ do not, in general, coincide with the principal axes of the defect, and the relative orientation of these two sets of axes should also be determined.

In the zeroth-order representation, $\mathbf{A}$ and $\mathbf{I}$ are quantized along $\mathbf{H}_0$, $\mathbf{K}$ is quantized along the molecular axis, and a 16-dimensional set of basis states is formed:

$$\psi(m_s,\mathbf{K},m_K,m_I)=|m_S\rangle|\mathbf{K},m_K\rangle|m_I\rangle. \tag{6}$$

For the magnetic field parallel to the Z axis, the zeroth-order solution to Eq. (1) is

$$E(m_s,\mathbf{K},m_K,m_I)=g_Z\beta_0\mathbf{H}_0m_s+g_0\beta_0\mathbf{T}_Zm_sm_K -\gamma_Fh\mathbf{H}_0m_K+hWm_Im_s-\gamma_nh\mathbf{H}_0m_I, \tag{7}$$

where W is a function of $\mathbf{A}_x$, $\mathbf{A}_y$, and $\mathbf{A}_z$ and directional cosines.[19,20] From Eq. (7), ENDOR transition frequencies, which are determined by the selection rules $\Delta m_I=\pm1$, $\Delta m_s=\Delta m_K=0$, are

$$\nu_{\mathrm{ENDOR}}=\gamma_n\mathbf{H}_0\pm\tfrac{1}{2}W, \quad \text{if} \quad \gamma_n\mathbf{H}_0>\tfrac{1}{2}W \tag{8}$$

$$\nu_{\mathrm{ENDOR}}=\tfrac{1}{2}W\pm\gamma_n\mathbf{H}_0, \quad \text{if} \quad \gamma_n\mathbf{H}_0<\tfrac{1}{2}W. \tag{9}$$

The $\pm$ signs correspond to the electron spin states $m_s=\mp\frac{1}{2}$ for $W>0$. Expression (8) holds for all nuclei reported here except those of shell B. These frequencies, which occur in pairs, are exact only when the magnetic field is parallel to a principal axis of $\mathbf{A}$ that is also parallel to a principal axis of $\mathbf{T}$.

The large anisotropic ESR hyperfine interaction results in large off-diagonal elements in the spin Hamiltonian of Eq. (1).[20,28] These off-diagonal elements, which depend on the nuclear spin state of the ESR fluorines, introduce large perturbations. In order to correctly predict the dependence of the ENDOR on the ESR lines, the complete spin Hamiltonian must be constructed and diagonalized.

In constructing the complete ENDOR Hamiltonian matrix for an exact solution, it is necessary to introduce two coordinate systems: X, Y, Z, which refer to the principal axes of $\mathbf{T}$, which are labeled $X\|[\bar{1}10]$, $Y\|[\bar{1}\bar{1}2]$, $Z\|[111]$[30]; and x, y, z, which refer to the principal axes of $\mathbf{A}$. In general, x, y, z are related to X, Y, Z through a set of Euler angles. For all but three shells (G, I, and L), the YZ plane is a principal plane of the hyperfine interaction by symmetry. Then a single angle θ, which specifies the orientation of the principal axes of $\mathbf{A}$ within the principal plane, is required. For the three shells that do not have a principal plane determined by symmetry, the plane that contains the ENDOR

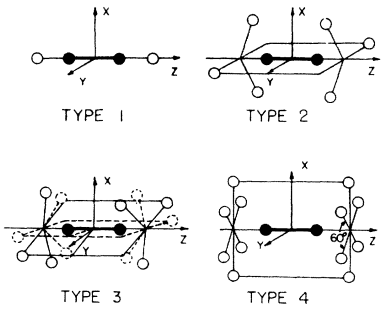

FIG. 8. Shell types of the symmetry of the ⟨111⟩ defect. A principal plane is also shown for those nuclei which are contained in it. For type 3, the angle between the solid or dashed plane and the Y axis is 19.11°.

[28] I. Bass and R. L. Mieher, Phys. Rev. Letters **15**, 25 (1965); Phys. Rev. **175**, 421 (1968).

[29] A maximum splitting of about 120 kc/sec was observed for the fluorine nuclei of shell B which are related by inversion. This second-order hyperfine structure has been observed previously in the ENDOR of the F center. W. E. Blumberg and G. Feher, Bull. Am. Phys. Soc. **5**, 183 (1960); see also Ref. 19.

[30] Because of the axial symmetry of the ESR, the choice of X and Y is not unique. In the ENDOR analysis it is convenient to specify the orientation of these axes as given in Fig. 1.

nucleus, and the axis of the F_2^- is taken as a principal plane.[31] By using this assumption, good fits with the ENDOR data were obtained for these three shells. A principal plane for nuclei in shell G (type 4) and shells I and L (type 3) is shown in Fig. 8. In this case, an additional angle φ (determined by geometry) specifies the angle between this principal plane and the YZ plane (for shell G, $\varphi=90°$; for shells I and L, $\varphi=19.11°$).

The matrix diagonalization procedure has been discussed in detail elsewhere.[28] Only a brief outline will be given here. The same basis states which were formed for the zeroth-order solution [Eq. (6)] are used. Numerical values for $\mathbf{g}$ and $\mathbf{T}$, which were determined from the ESR study, are substituted into the matrix. The matrix is diagonalized and ENDOR transition frequencies are calculated. The ENDOR hyperfine constants A_x, A_y, A_z, and θ are varied to obtain the best fit with the experimental spectrum of the ENDOR for each lattice shell.

C. Symmetry Considerations

The angular dependence of the ENDOR hyperfine interaction reflects the symmetry of the defect. Symmetry considerations are fundamental in assigning a set of ENDOR lines to a corresponding set of lattice nuclei. The ⟨111⟩ defect, as mentioned earlier, has rhombohedral symmetry (C_{3v}). The ⟨111⟩ axis is a three-fold rotation axis, and there are three {110} reflection planes which contain the ⟨111⟩ axis. The defect and lattice have a twofold rotation axes perpendicular to each of the three reflection planes. Also, there is inversion symmetry through the center of the F_2^- molecule.

In discussing ENDOR it is convenient to introduce the concept of lattice shells. Lattice shells are groups of lattice nuclei which transform into one another through the symmetry operations of the defect. Each nucleus in a shell has the same principal values for the hyperfine tensor $\mathbf{A}$, and the principal axes of $\mathbf{A}$ must transform into each other by the symmetry operations of the defect. Nuclei within a shell are said to be equivalent if their principal axes make the same angle with $\mathbf{H}_0$. A single ENDOR line is expected from equivalent nuclei if the interaction between the equivalent nuclei is small.[29] If the defect has ⟨111⟩ symmetry, all nuclei in the same shell are equivalent when $\mathbf{H}_0$ is parallel to the ⟨111⟩ axis.

For the ⟨111⟩ defect, it is convenient to group the shells into types. Each shell of a particular type displays the same local symmetry and have similar ENDOR patterns. In Fig. 8 four different shell types for the ⟨111⟩ defect are shown. The symmetry properties for 13 lattice shells are listed in Table I. The shell structure is more complex for more distant lattice nuclei.

As mentioned earlier $\mathbf{H}_0$ is rotated in the $(\bar{1}10)$ plane. Those nuclei that are related by reflection through this plane remain equivalent for all orientations of $\mathbf{H}_0$. If a nucleus is contained in this plane, symmetry requires that one of the principal axes of the nucleus must be perpendicular to this plane (i.e., along X). If a nucleus is on a twofold rotation axis, this axis is a principal axis for the nucleus. If a nucleus is on an axis of threefold rotational symmetry, then the hyperfine interaction has axial symmetry. Formal aspects of these symmetry considerations are based on the fact that the spin Hamiltonian [Eq. (1)] must be invariant under the symmetry operations of the ⟨111⟩ defect. Such considerations allow one to predict the principal axes that are determined by symmetry and the expected number of ENDOR lines for each shell.

TABLE I. Symmetry properties of lattice shells. The principal axes are given for the listed nuclear site.

Shell	No. of nuclei in shell	Shell type	Principal axis by symmetry	Nuclear site	Ratio of equivalent nuclei for {110} rotation
A(Li)	6	2	X	YZ plane	1-2
B(F)	6	2	X	YZ plane	1-2
C(Li)	2	1	X, Y, Z	Z axis	1
D(F)[a]	6	4	X	X axis	1-2
E(Li)	6	2	X	YZ plane	1-2
F(F)	6	2	X	YZ plane	1-2
G(Li)	12	4	none	XZ plane	1-1-1
H(F)	6	2	X	YZ plane	1-2
I(Li)	12	3	none	±19.11° from YZ plane	1-1-1
J(F)	6	2	X	YZ plane	1-2
L(F)	12	3	none	±19.11° from YZ plane	1-1-1
N(F)[a]	6	2	X	YZ plane	1-2
P(F)	2	1	X, Y, Z	Z axis	1

[a] Shells D and N are degenerate cases of types 4 and 2, respectively, since all the nuclei are in the XY plane.

V. RESULTS AND DISCUSSION

A. ENDOR

The above symmetry considerations have permitted the correlation of 11 lattice shells with sets of ENDOR lines. The ENDOR hyperfine constants obtained by fitting to the spin Hamiltonian are listed in Table II. The assignment of $\mathbf{A}_x$, $\mathbf{A}_y$, and $\mathbf{A}_z$ was made so that the angle between the principal axes of $\mathbf{A}$ and the corresponding principal axes[30] of $\mathbf{T}$ (i.e., X, Y, and Z) was acute. The listed hyperfine constants refer to the positions of the subscripted nuclei (e.g., A_1) in Fig. 1.

In the study of other F_2^--type centers by ENDOR, it was found that one of the principal axes (not determined by symmetry) is oriented approximately towards the nearest fluorine of the F_2^-. This fact was particularly helpful in identifying the ENDOR from the fluorine shells F, H, and J whose hyperfine constants all have about the same magnitude.

As a final check in identifying the lines, the dipole-dipole part of the hyperfine tensor [Eq. (3)] was calculated using the computer program developed by Daly and Mieher.[31] These calculations were particu-

[31] D. F. Daly and R. L. Mieher, Phys. Rev. Letters **19**, 637 (1967); Phys. Rev. **183**, 368 (1969).

TABLE II. The ENDOR hyperfine constants expressed in Mc/sec. θ is the angle between the z and Z axes and is positive for z rotated toward the Y or X axes (see Fig. 1). The principal axes are given for the subscripted nuclei in Fig. 1.

Shell	A_x	A_y	A_z	θ	a	B_x	B_y	B_z
A(Li)	−4.87±0.02	3.07±0.01	− 3.88±0.01	−17.5 ±0.5°	− 1.89	− 2.98	+ 4.96	− 1.99
B(F)	+9.50±0.50	62.70±2.00	10.80±0.20	29.5 ±2.0°	+27.7	−18.2	+35.0	−16.9
C(Li)	−1.54±0.01	− 1.54±0.01	1.80±0.01	0°	− 0.43	− 1.11	− 1.11	+ 2.23
D(F)	1.12±0.04	− 4.65±0.02	− 3.80±0.02	− 6.5 ±2.0°	− 2.44	+ 3.56	− 2.21	− 1.36
E(Li)	−0.71±0.03	1 20±0.02	− 0.51±0.02	−13.25±1.00°	− 0.01	− 0.70	1.21	− 0.50
F(F)	−1.25±0.03	2.00±0.01	− 1.14±0.02	−29.5 ±1.0°	− 0.13	− 1.12	2.13	− 1.10
G(Li)	0.76±0.02	− 0.38±0.02	− 0.37±0.02	−44.5 ±1.0°	0.00	+ 0.76	− 0.38	− 0.37
H(F)	−0.86±0.02	− 0.83±0.02	1.41±0.02	22.75±0.50°	− 0.09	− 0.77	− 0.74	+ 1.50
I(Li)	−0.32±0.02	+ 0.58±0.02	− 0.30±0.02	−12.0 ±1 0°	− 0.01	− 0.31	+ 0 58	− 0.21
J(F)	−0.46±0.04	− 0.42±0 02	1 46±0.02	−34.5 ±1.0°	+ 0.65	− 0.65	− 0.61	1.27
L(F)	−0.53±0.04	1.28±0.02	− 0.48±0.02	+24.0 ±1.0°	+ 0.09	− 0.62	+ 1.19	− 0.57

larly helpful for the distant nuclei whose ENDOR lines lie close to the central packet at $\gamma_n \mathbf{H}_0$ and whose ENDOR angular dependence is difficult to follow completely. For these distant nuclei, the contact interaction as well as the relaxation from the perfect lattice position is expected to be small, and hence the difference between the dipole-dipole calculations with the ENDOR nucleus at its perfect lattice position and the experimental hyperfine constants should also be small. The absolute signs of the hyperfine constants can not be determined from the experiment. The signs for $\mathbf{A}_x$, $\mathbf{A}_y$, and $\mathbf{A}_z$ have been chosen to agree with the theoretical principal values of $\mathbf{B}$. By using these calculations it was possible to identify the ENDOR of two additional lattice shells, N and P (See Figs. 1 and 3). The angular dependence of these two shells could not be followed enough to determine hyperfine constants.

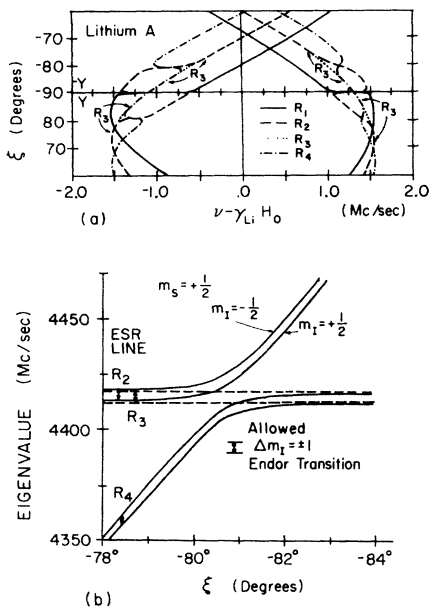

FIG. 9 (a) The angular dependence of the ENDOR of the lithium A nuclei contained in the (1̄10) plane near $|\xi|=90°$. The R_3 line which is a pure singlet does not mix with the other three lines. The effects of mixing the R_2 and R_4 ESR lines at $|\xi|=81°$ and the R_1 and R_2 ESR lines at $|\xi|=90°$ are shown. (b) The eigenvalues of the spin Hamiltonian for the $m_s=\frac{1}{2}$ state are shown near $\xi=-81°$. The energy of the R_1 ESR line is too large to fit on the scale. The eigenvalues are determined such that the ESR transition frequency for the R_3 ESR line is equal to the microwave frequency (8830 Mc/sec). The frequency scale is too large to show the crossing of the R_2 and R_3 ENDOR lines.

Shell D has the YZ plane as a principal plane. The observed rotation of the principal axes in this plane by $\theta=-6.5°$ from the Z axis is a measure of the effect of the lattice on the F_2^- wave function. If lattice effects are neglected, symmetry would require the hyperfine principal axes to be along Y and Z. For the more distant shell G, this rotation was not observed within experimental error.

Also listed in Table II are the Fermi contact interaction a and principal values of the dipole-dipole tensor $\mathbf{B}$. As in the case of the other F_2^--type defects, the contact interaction is negative for most of the shells. The negative contact interaction has been explained qualitively as arising from exchange polarization of the closed shell orbitals of the F_2^- wave function.[20,31]

The diagonalization of the spin-Hamiltonian matrix yields the correct dependence of the ENDOR on the nuclear-spin states of the molecular fluorine. The largest perturbations on the ENDOR occur when $\xi>70°$. It was not possible to observe these effects on the R_4 ESR line directly, because of the large F and V_K concentration and the general weakening of the ENDOR signal in this region. The ability of the matrix diagonalization procedure to predict higher-order perturbation effects has been demonstrated for the case of the V_K center.[27]

The angular dependence of the lithium A ENDOR that was taken on the R_1 and R_4 ESR lines is shown in Fig. 7. The predicted angular dependence of the ENDOR of the R_3 ($K, m_K=0, 0$) ESR line, which is not affected by the ESR hyperfine interaction, is also shown for comparison. At $\xi=\pm 90°$, the ENDOR from equivalent nuclei must be equal, and in some cases the spin Hamiltonian predicts an abrupt change in the

ENDOR frequency between $\xi=\pm 89.5°$ and 90° to satisfy this requirement [see Fig. 9(a)]. The matrix diagonalization analysis predicts an unusual behavior for all lattice shells for the angular dependence $|\xi|=81°$ for the ENDOR of the R_4 line. This phenomenum is due primarily to interaction between the R_4 (K, $m_K=1, 1$) and R_2 ($K, m_K=1, 0$) ESR energy levels. It can be thought of as antilevel crossing which occurs when small off-diagonal elements in the Hamiltonian matrix (in this case, T_Y) mix energy levels corresponding to different nuclear-spin states of the F_2^-.[29] The energy-level scheme is illustrated in Fig. 9(b). At $|\xi|\cong 81°$, the R_2 and R_4 ESR lines both contain equal admixture of the $|K,m_K\rangle=|1,1\rangle$ and $|1,0\rangle$ spin states. For $|\xi|>81°$, the R_2 ESR line contains primarily $|1,1\rangle$ character, while the R_4 ESR line contains primarily $|1,0\rangle$ character. The R_2 ESR line in this region is an extension of the R_4 ESR line, and vice versa. At $\xi=90°$, the R_1 and R_2 lines are also mixed and both lines contain almost equal mixtures of the $|1,-1\rangle$ and $|1,1\rangle$ nuclear-spin states of the F_2^-. The mixing of the spin states appear as a crossing of the R_2 and R_4 ENDOR lines. A similar behavior occurs near 90° between the R_1 and R_2 ENDOR lines. This effect also occurs in the ENDOR of the V_K type centers.[27,28]

B. ESR And ENDOR Correlation

As mentioned earlier, a resolved secondary splitting is observed in the ESR spectra. The angular dependence of the secondary splitting is complicated. The large ENDOR hyperfine constants for the shell B nuclei suggests that they are responsible for the secondary splitting. For $\mathbf{H}_0\|[111]$, all six fluorine B nuclei, which have spin $\frac{1}{2}$, are equivalent and could produce a seven-line splitting of the ESR. The $R_1(0)$ line does show a seven-line partially resolved splitting with a separation of 12 G between each line (see Fig. 2). As $\mathbf{H}_0$ is rotated towards the [110] direction, the secondary splitting is composed of three lines which indicate a predominant interaction with the two equivalent shell B fluorine nuclei that lie in the $(\bar{1}10)$ plane. As $\mathbf{H}_0$ is rotated toward the [001] direction, the splitting is composed of five lines, which arises from the interaction with the four equivalent shell B fluorine nuclei that do not lie in the $(\bar{1}10)$ plane.

TABLE III. Correlation of the ENDOR with the resolved secondary splitting of the ESR.

ESR line	ESR splitting (lines)	W (ESR) (Mc/sec)	W (ENDOR) (Mc/sec)
$R_1(0°)$	7	34	34.7
$R_1(30°)$	5	40	42.0
$R_4(-35.3°)$	3	57	62.3[a]
$R_1(-70.5°)$	3	64	62.3[a]

[a] These values are accidently equal for this accuracy.

From Eq. (9), it is evident that the quantity $\nu(m_s=\frac{1}{2})+\nu(m_s=-\frac{1}{2})$ is a measure of W, where W is now the total hyperfine interaction that includes any perturbation effects included in the spin Hamiltonian or otherwise. To make a quantitative comparison between the ESR and the ENDOR, values of W as measured by ESR and ENDOR are compared. This comparison is made in Table III for cases where the secondary splitting of the ESR could be reliably measured. The correlation between W (ESR) and W (ENDOR) shows that the resolved secondary splitting is due to the shell B fluorines.

C. Conclusion

From the ESR study it was possible to determine that the structure of this new defect is a molecule ion F_2^- and that the orientation of the molecular axis is along $\langle 111\rangle$. From the ENDOR study it is determined that the F_2^- is located on a single negative-ion lattice site. The correlation of 13 nonequivalent lattice shells with ENDOR lines firmly establishes the model of the defect.

Since no splittings of the ENDOR lines are observed,[11,28] this $\langle 111\rangle$ defect is the "pure" interstitial, in the sense that no other defects or impurities are located within several lattice constants. Therefore, the intrinsic interstitial fluorine atom takes the form of a negatively charged diatomic molecule that is localized on a single negative-ion lattice site and oriented in a $\langle 111\rangle$ direction.